

Oblateness, Radius, and Mean Stratospheric Temperature of Neptune from the 1985 August 20 Occultation

W. B. HUBBARD

Lunar and Planetary Laboratory, University of Arizona, Tucson, Arizona 85721

PHILIP D. NICHOLSON

Astronomy Department, Cornell University, Ithaca, New York 14853

EMMANUEL LELLOUCH,¹ BRUNO SICARDY,² AND ANDRÉ BRAHIC²

Observatoire de Paris, 92190 Meudon, France

FAITH VILAS³

NASA Johnson Space Center, Houston, Texas 77058

PATRICE BOUCHET

European Southern Observatory, La Silla, Chile

ROBERT A. McLAREN

Canada-France-Hawaii Telescope Corporation, Kamuela, Hawaii 96743

ROBERT L. MILLIS AND LAWRENCE H. WASSERMAN

Lowell Observatory, Flagstaff, Arizona 86001

J. H. ELIAS,⁴ K. MATTHEWS,⁴ AND J. D. MCGILL

Physics Department, California Institute of Technology, Pasadena, California 91125

AND

C. PERRIER²

Observatoire de Lyon, 69230 Saint Genis Laval, France

Received February 19, 1987, revised June 17, 1987

The occultation of a bright ($K \sim 6$) infrared star by Neptune revealed a central flash at two stations and provided accurate measurements of the limb position at these and several additional stations. We have fitted this data ensemble with a

¹ Present address: ESTEC, 2200 AG Noordwijk, Netherlands.

² Visiting astronomer, Canada-France-Hawaii Telescope, operated by the National Research Council of Canada, the Centre National de la Recherche Scientifique of France, and the University of Hawaii.

³ Visiting astronomer, Cerro Tololo Inter-American Observatory, supported by the National Science Foundation under Contract No. AST 78-27879.

⁴ Visiting astronomer at the Infrared Telescope Facility, which is operated by the University of Hawaii under contract to the National Aeronautics and Space Administration.

general model of an oblate atmosphere to deduce the oblateness e and equatorial radius a_0 of Neptune at the 1- μ bar pressure level, and the position angle p_n of the projected spin axis. The results are $e = 0.0209 \pm 0.0014$, $a_0 = 25269 \pm 10$ km, $p_n = 20.1^\circ \pm 1^\circ$. Parameters derived from fitting to the limb data alone are in excellent agreement with parameters derived from fitting to central flash data alone (E. Lellouch, W. B. Hubbard, B. Sicardy, F. Vilas, and P. Bouchet, 1986, *Nature* 324, 227–231), and the principal remaining source of uncertainty appears to be the Neptune-centered declination of the Earth at the time of occultation. As an alternative to the methane absorption model proposed by Lellouch *et al.*, we explain an observed reduction in the central flash intensity by a decrease in temperature from 150 to 135°K as the pressure rises from 1 to 400 μ bar. Implications of the oblateness results for Neptune interior models are briefly discussed. © 1987 Academic

Press, Inc.

INTRODUCTION

The occultation by Neptune on 1985 August 20 of star 39 on the prediction list of Nicholson, Matthews, and Gilmore (P. Nicholson, K. Matthews, and G. Gilmore 1985, private communication) yielded data at higher signal/noise (S/N \sim 100 at 0.1-sec time resolution, for the Chile observations) than for any previous Earth-based stellar occultation by a planet. Observations were successfully obtained at six stations, which are listed in Table I. All of the experiments were carried out at *K*-band (2.2 μ m), except for the Lowell experiment, where data were taken at 0.8 μ m.

In Table I, CTIO denotes Cerro Tololo Inter-American Observatory at La Serena, Chile; ESO denotes European Southern Observatory at La Silla, Chile; IRTF denotes the NASA Infrared Telescope Facil-

ity at Mauna Kea, Hawaii; CFHT denotes the Canada–France–Hawaii Telescope at Mauna Kea; Lowell denotes the Perkins telescope at Lowell Observatory; and Mt. Wilson denotes the 0.6-m telescope at Mt. Wilson Observatory, California. All of the stations successfully observed both immersion and emersion. In addition, CTIO and ESO observed the enhanced stellar signal near midoccultation produced by global focusing by Neptune (Lellouch *et al.* 1986, Paper I)—the so-called central flash.

Paper I derived the oblateness of Neptune e and the transmission factor for the Neptune atmosphere at the level probed by the central flash by fitting the central flash data with a model of an oblate, isothermal atmosphere with scale height H_f . The parameters of the model of Paper I were e , the scale height at the level probed by the central flash H_f (the ratio of H_f to the true

TABLE I
STATION DATA

Station	Observer(s)	Latitude	East longitude	Altitude (m)	Aperture (m)
CTIO	Vilas	–30°09′56.3″	–70°48′54.5″	2225	1.5
ESO	Bouchet	–29°15′21.0″	–70°43′53.7″	2347	1.0
IRTF	Elias	19°49′34.0″	–155°28′15.0″	4100	3.0
CFHT	Sicardy <i>et al.</i>	19°49′41.9″	–155°28′18.0″	4204	3.6
Mt. Wilson	Matthews	34°12′59.5″	–118°03′34.95″	1742	0.6
Lowell	Millis	35°05′48.6″	–111°32′09.3″	2198	1.8

Note: IRTF and CFHT coordinates are from the respective observer's manuals. Their relative positions contain errors which are negligible for the purposes of this paper.

scale height at the central flash level is equivalent to the transmission factor), the coordinates x_0, y_0 of the projected geometrical center of Neptune in the sky plane, and the projected position angle of Neptune's north pole in the sky plane, p_n . The model was also dependent on the equatorial radius of Neptune a_0 and the Neptune-centered declination of the Earth, β_e , but these parameters could be described in advance as the model was very insensitive to a_0 , while the dependence on β_e could be scaled from the derived value of e .

The objective of this paper is to carry out a solution for the full set of parameters e, x_0, y_0, p_n , and a_0 by simultaneously fitting to the limb profile of Neptune as defined by the immersion and emersion occultation data, as well as to the central flash intensity pattern observed at ESO and CTIO. We also derive a mean atmospheric temperature profile in the pressure range covered by the data which is consistent with the observations. Comparison of the results from separate fits to the limb profile and to the central flash pattern provides a further consistency check and test of the adequacy of the model. The two separate fitting procedures are partially overlapping and partially complementary. Thus, the limb profile strongly constrains e, x_0, y_0 , and a_0 (as well as H_0 , the scale height at the 1- μ bar pressure level), but is insensitive to p_n and independent of H_f . The central flash intensity pattern, as measured at the two stations, strongly constrains e, x_0, y_0, H_f , and p_n , but is insensitive to a_0 . Neither fitting procedure provides a meaningful constraint on β_e , which must be derived from independent information.

IMMERSION AND EMERSION TIMINGS

The limb profile of Neptune was computed from the calculated times of half intensity of the star signal as observed from each station. The procedure for computing the half-intensity times at CTIO and ESO was as follows. First, a polynomial in time t was fitted to the combined star and planet signal over the entire night's observations,

excluding the interval of actual stellar occultation by the planet. Then, the planetary fraction of this combined signal was estimated from the depth of the occultation and used to construct a preliminary stellar signal normalized to the unocculted value, $\phi(t)$. This signal was compared with the central flash data, and the planetary background signal was adjusted for self-consistency with the central flash data. Then this planetary background signal was used to renormalize the stellar signal once again. The resulting normalized stellar signal $\phi(t)$ was then fitted with a Baum-Code function $\phi_{BC}(t)$ to derive the parameters $t_{1/2}$ and v_{\perp}/H_0 , where $t_{1/2}$ is the time at which the average stellar signal reaches one-half of its unocculted value ($\phi = \frac{1}{2}$), and v_{\perp}/H_0 is the ratio of the component of the star's velocity in the sky plane perpendicular to the planetary limb (and into the shadow) to the scale height H_0 at the immersion/emersion level (which may differ from the scale height H_f at the level which forms the central flash, some 250–300 km deeper in Neptune's atmosphere).

Half-intensity times at the other stations, for which central flash data were not available, were for the most part obtained using similar procedures. However, the unocculted and "fully occulted" levels were derived by suitable averages of intervals where the combined star and background signals were essentially constant. Further discussion of possible problems with this procedure is given below. IRTF half-intensity times were determined by a simultaneous four-parameter fit to $H_0, t_{1/2}$, planet-only signal, and star-only signal. Mt. Wilson times were estimated by eye from a strip chart.

Table II presents half-intensity times at the six stations. Also tabulated, for CTIO and ESO only, are the times of peak central flash. The central flash times at CTIO and ESO were determined by fitting a Gaussian profile to the data in the immediate vicinity of the central flash maximum intensity, and not from a general fit to the overall central intensity profile.

TABLE II
TIMES OF IMMERSION AND EMERSION (HALF
INTENSITY) AND PEAK CENTRAL FLASH

Station	Immersion	Central flash	Emersion
CTIO	5 ^h 17 ^m 31.57 ± 0.32	5 ^h 55 ^m 21.12 ± 0.32	6 ^h 34 ^m 59.99 ± 0.32
ESO	5 ^h 17 ^m 26.58 ± 0.32	5 ^h 55 ^m 19.51 ± 0.32	6 ^h 34 ^m 55.54 ± 0.32
IRTF	5 ^h 28 ^m 17.77 ± 0.32		6 ^h 41 ^m 16.66 ± 0.32
CFHT	5 ^h 28 ^m 16.77 ± 0.32		6 ^h 41 ^m 17.76 ± 0.32
Mt. Wilson	5 ^h 23 ^m 05.5 ± 5 ^s		6 ^h 36 ^m 17.5 ± 5 ^s
Lowell	5 ^h 22 ^m 18.54 ± 1.32		6 ^h 35 ^m 43.99 ± 1.32

To compute the corresponding occultation points on the sky plane, we constructed a Cartesian coordinate system, with x representing the east–west component of an occultation point’s separation from the ephemeris center of Neptune (with x increasing to the east) and y the north–south component (with y increasing to the north). The procedure for computing the location of the occultation tracks in the sky plane is described (for example) in Hubbard *et al.* (1985). The ephemeris of apparent positions for Neptune was kindly provided by Standish (E. M. Standish, Jr. 1986, private communication) and is identical to that published in the 1985 *Astronomical Almanac* (corresponding to JPL ephemeris DE-120), except that one additional significant figure was added to each coordinate to reduce interpolation errors to an acceptable level. A constant offset x_0 , y_0 in the sky plane was then added to Neptune’s apparent ephemeris position in order to bring the relative positions of Neptune and the star

into conformity with the fit to the observations. The coordinates x and y were measured from the corrected Neptune center in the sky plane.

In order to compare the apparent star positions with apparent Neptune ephemeris on the J2000 (DE-120) system, the star position on the older B1950 system ($\alpha_{1950.0} = 18^{\text{h}}02^{\text{m}}07^{\text{s}}.186$, $\delta_{1950.0} = -22^{\circ}18'10''.02$) must be first converted to the newer J2000 system (Standish 1982). This conversion was carried out using the procedures documented on page x of the 1985 *Astronomical Almanac*, and then the apparent star positions were computed using the Besselian day numbers in the same reference. Table III gives the resulting apparent geocentric star and planet positions for a 5-day interval centered on the occultation.

Comparing the station coordinates for IRTF and CFHT (Table I) with the corresponding half-intensity times for these stations given in Table II, we note that the derived times are discrepant by 1 sec for both immersion and emersion, but the telescope coordinates are within 300 m of each other, which could account for a time difference of no more than 0.03 sec. This problem was carefully investigated by comparing the arrival times of strong fluctuations in the stellar intensity (“spikes”) at the two stations. As would be expected for such a small separation, the fluctuations correlate in detail between the two stations. But arrival time differences (IRTF – CFHT) were +0.16 sec for immersion and

TABLE III
APPARENT GEOCENTRIC POSITIONS OF NEPTUNE AND THE OCCULTED STAR AT 0^h EPHEMERIS
TIME ON THE DATES GIVEN (J2000 SYSTEM)

Date	α (Neptune)	δ (Neptune)	L	α (star)	δ (star)
August 18	18 ^h 4 ^m 23 ^s .6712	–22°18′0.2400″	29.646071179	18 ^h 4 ^m 16 ^s .4104	–22°18′6.7360″
August 19	18 ^h 4 ^m 20 ^s .3501	–22°18′3.0730″	29.659911554	18 ^h 4 ^m 16 ^s .3915	–22°18′6.7790″
August 20	18 ^h 4 ^m 17 ^s .1507	–22°18′5.8800″	29.673918841	18 ^h 4 ^m 16 ^s .3719	–22°18′6.7931″
August 21	18 ^h 4 ^m 14 ^s .0766	–22°18′8.6640″	29.688088504	18 ^h 4 ^m 16 ^s .3539	–22°18′6.7792″
August 22	18 ^h 4 ^m 11 ^s .1310	–22°18′11.4320″	29.702415992	18 ^h 4 ^m 16 ^s .3394	–22°18′6.7470″

Note: L is true geocentric distance to Neptune in AU.

+0.28 sec for emersion, with an uncertainty of about 0.04 sec, suggesting a small absolute timing discrepancy and perhaps also a rate discrepancy on the order of a part in 10^5 . It is likely that errors in CFHT timings are primarily responsible for the differences, as the IRTF data included timing signals from the National Bureau of Standards satellite receiver inserted directly at the start and end of the data tape.

The remainder (and more important part) of the discrepancy in times appears to be attributable to a systematic difference in the derived stellar intensities, probably resulting from differences in derived full-intensity and zero-intensity baselines. Near half intensity, the derived IRTF intensities are systematically larger than those at CFHT by 1 and 3% at immersion and emersion, respectively, which in turn could account for 0.4 and 1.1 sec of the half-intensity time differences, respectively, in the same sense as the observed residuals. There appears to be no unambiguously correct resolution of the discrepancies, and so the unaltered timings have been used in the analysis. This procedure appears to be permissible because of the quality and redundancy of the entire data set. However, this problem provides a warning that even with occultation data of the excellent quality available here, unavoidable systematic errors in lightcurve normalizations may lead to true uncertainties in half-intensity times which exceed by a substantial factor the formal uncertainties resulting from lightcurve fits.

SOLUTIONS AND PROCEDURES

Solutions 1 and 2

Our preferred solution, which is based on a simultaneous fit to the central flash data (ESO and CTIO) and the immersion/emersion data at three stations (ESO, CTIO, and CFHT) is denoted as solution 1. This solution makes use of the high-quality ESO and CTIO data sets which cover chords with a closest-approach distance approximately

1100 km south of the shadow center, together with the CFHT data set which covers a chord with a closest-approach distance 5900 km north of the center (the IRTF data set is redundant for this chord, as explained). Solution 2 fits only to the ESO and CTIO central flash data, as in Paper I. Solution 3, which calculates the best-fit limb profile using only the half-intensity times from all six stations, is presented in the next subsection.

Solution 1 makes no use of the half-intensity times presented in Table II. Instead, the solution yields model lightcurves which simultaneously fit the central flash occultation data and the limb occultation data. The parameters of the model are the corrections to adopted background levels for ESO, CTIO, and CFHT, the previously defined parameters e , x_0 , y_0 , p_n , H_0 , a_0 , and a new parameter γ , which represents a linear correction to the model lightcurve for a constant scale height, and which is intended to represent the effects of temperature varying with altitude. That is, if we let $\phi_{BC}(\zeta)$ be the Baum-Code function for a displacement ζ in the shadow plane, where $\zeta (=v_{\perp}[t - t_{1/2}]/H_0)$ near the limb is the observer's distance into the shadow from the half-intensity limb in units of H_0 , then the model lightcurve (before corrections for focusing due to limb curvature) is assumed to be given by

$$\phi_{mod} = \phi_{BC} \quad (1)$$

for $\zeta < 0$, and by

$$\phi_{mod} = \phi_{BC}(1 - \gamma\zeta) \quad (2)$$

for $\zeta \geq 0$. For very small γ , as we derive here ($\gamma = 6 \times 10^{-4}$), the model lightcurve near the limb is essentially identical to the Baum-Code lightcurve. But near the shadow's center, where $\zeta \sim 500$, the intensity is reduced by about 30% with respect to the Baum-Code value, as is strongly required by the data set (see Paper I). Once γ has been derived, the final step is to invert the lightcurve ϕ_{mod} to obtain either a temperature profile (assuming no absorption) or an

absorption profile (assuming constant temperature). Paper I presented results for possible methane abundances in Neptune's upper atmosphere which could yield sufficient absorption to account for the reduced central flash intensity. In the present solution, we derive instead a temperature profile corresponding to a model lightcurve of the form given by Eq. (2), with no absorption along the optical path.

We found that it was desirable to carry out solution 1 using a two-step process. The data sets can be divided into three domains: (a) the limb region within about $0.2 a_0$ from the limb; (b) the central flash region within about $0.15 a_0$ from the midpoint of the data (ESO and CTIO only); and (c) the remaining region where the star signal varies only slightly and has an average value $\langle \phi \rangle \sim 8 \times 10^{-3}$. If a fit is carried out simultaneously to all three domains, domain (c) has a disproportionate effect in relation to its information content because of the large number of data points and the relatively low signal/noise ratio.

We therefore first adopted a preliminary set of parameters and calculated a model stellar intensity function for the three stations. The model and data were then compared in domain (c) and the background levels for the three stations were adjusted until the average intensity for model and data in domain (c) was in agreement for all data sets. With the background levels held constant, the model parameters were then adjusted to achieve a simultaneous least-squares best fit in the intensity at all three stations for domains (a) and (b). With the resulting new parameters, we then returned to the initial procedure for adjusting the background levels, and the iterations proceeded until satisfactory convergence was achieved. This procedure required only about five iterations for satisfactory convergence and was quite stable. Table IV presents parameters for solution 1. Note that the value of p_n (20.1°) is derived from the overall fit to the central intensity pattern and differs by about one probable error

TABLE IV
PARAMETERS OF SOLUTIONS 1 AND 2

Parameter	Solution 1	Solution 2
Apparent oblateness ($e' = e \cos^2 \beta_e$)	0.0172	0.0179
e (for $\beta_e = -25.0^\circ$)	0.0209	0.0218
x_0	+2454 km ($\Delta\alpha = +0.123''$)	
y_0	-6028 km ($\Delta\delta = -0.280''$)	
Δx_0		-21 km
Δy_0		-19 km
p_n	20.1°	20.1°
H_0	51.5 km	
H_f		35 km
a_0	25,269 ^a km	
γ	6.2×10^{-4}	

^a Includes ray deflection corrections of H_0 for refraction and 54 km for relativistic bending.

from the position angle which would be calculated from the peak central flash times presented in Table II, 19.3° . The discrepancy between the two values is consistent with the probable error assigned to p_n . Because the central flash observed at the two stations defines an "optical axis" which virtually coincides with the planet's projected rotation axis, two-station observations of the flash close to the central evolute pattern provide a much more sensitive determination of p_n than observations of the limb profile alone.

In all three solutions presented in this paper (1, 2, and 3), the projected outline of Neptune on the plane of the sky is taken to be an ellipse with semimajor axis a_0 and semiminor axis $a_0(1 - e')$, where the apparent oblateness e' is related to the true oblateness e by $e' = e \cos^2 \beta_e$. This equation is valid to order e ; neglect of terms of order e^2 is justified because of the smallness of e , because the figure of Neptune is not an ellipse to order e^2 , and because a simple linear relation between e and e' eliminates the need for assumptions about the internal structure of Neptune in obtaining the "de-projected" oblateness of the planet. The semimajor and semiminor dimensions of Neptune's shadow are taken to be equal to a_0 and $a_0(1 - e')$, respectively, reduced by the scale height H_0 and the general-relativistic deflection of 54 km.

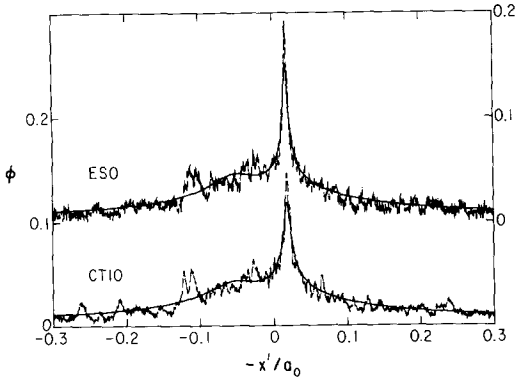


FIG. 1. Normalized stellar intensities computed from solution 1 (smooth continuous curves) compared with data, at ESO and CTIO, in the region of the central flash.

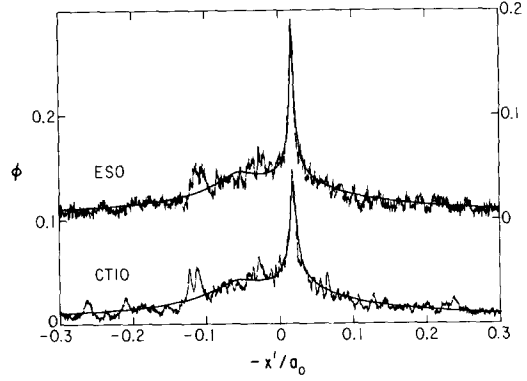


FIG. 2. Normalized stellar intensities computed from solution 2 (smooth continuous curves) compared with data, at ESO and CTIO, in the region of the central flash.

Figure 1 shows plots of model intensities from solution 1 and data in the vicinity of the central flash. The abscissa (x'/a_0) is defined such that x' represents the Cartesian coordinate of a station on the sky plane along a track parallel to the mean ESO and CTIO tracks, with the origin of the x' , y' coordinate system at the center of the planet. Thus $x' = 0$ when a station makes its closest approach to the center. The x' , y' axes are rotated to the west (i.e., to a negative position angle) with respect to the celestial x , y axes by 2.91° . The x' axis increases to the east.

Solution 2 is essentially a repetition of the solution presented in Paper I, but with some of the parameters and procedures adjusted slightly for consistency with the other two solutions of this paper. For this solution, we carried out a simultaneous least-squares fit to the ESO and CTIO central flash data in the region of the central flash, that is, for points on the chords which are within $0.3 a_0$ of the planet's center. The ESO and CTIO background levels and the planetary radius determined in solution 1 (reduced by 300 km) were used in solution 2. As in Paper I, the Baum-Code model lightcurve corresponding to a constant scale height H_f was used without modification to compute the central flash profile.

The adjustable parameters of solution 2 were thus e , Δx_0 , Δy_0 , p_n , and H_f , where Δx_0 , Δy_0 are the additional corrections to the position of the planetary center, to be added to the values x_0 , y_0 obtained from solution 1 (Table IV). Results from this procedure are presented in Table IV, and Fig. 2 shows a plot of the best-fit model intensities and the data, analogous to Fig. 1. Note that solution 2 fits the peak central flash intensity better than solution 1, as would be expected since solution 2 makes no attempt to fit the limb data, but it otherwise differs insignificantly from solution 1.

Figure 3 shows a possible profile of temperature versus altitude in the Neptune atmosphere. This profile is obtained by applying standard inversion techniques to the model intensity profile given by Eq. (2), with the value of γ given in Table IV. Note that although the model intensity profile has an intensity which is reduced by about 30% with respect to the Baum-Code value deep in the occultation, the corresponding temperature reduction is much more modest. Figure 4 shows the temperature-pressure profile in Neptune's atmosphere. These profiles are not true inversions of the intensity data, and their details are sensitive to the precise form of ϕ_{mod} . They are intended

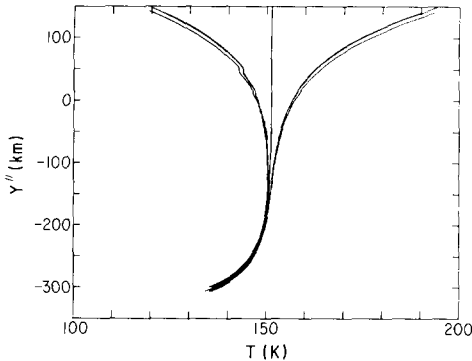


FIG. 3. Variation of temperature T with altitude Y'' above the half-intensity ($1\text{-}\mu\text{bar}$) level, as obtained from inverting Eq. (2). Different curves show the effects of arbitrary assumptions about the temperature at the starting level for the inversion and above that level.

only to show that the overall central flash intensity can be reduced by the required amount with a plausible temperature distribution. We have experimented with an alternative version of ϕ_{mod} , which has a step function that drops the intensity by 30% deep in the occultation. The alternative model yields a mean temperature profile which differs in its details from that in Fig. 4, but the deepest point (corresponding to the central flash region) again passes close to the values shown at the bottom of Fig. 4: $T = 135^\circ\text{K}$ at a pressure of $370\ \mu\text{bar}$, indicating that this point is reasonably model independent.

A recent model of Neptune's atmosphere, based on observations of the disk at $7\text{--}14$ and $17\text{--}23\ \mu\text{m}$ (Orton *et al.* 1987), obtains results which are very similar to those presented in Figs. 3 and 4. Specifically, the Orton *et al.* atmospheric model has a temperature of 144°K at $1\ \mu\text{bar}$ pressure, with a temperature decline to 138°K at $400\ \mu\text{bar}$, $277\ \text{km}$ deeper. However, the model of Orton *et al.* assumes that the methane mixing ratio in the stratosphere is in local saturation equilibrium, unaffected by a possible tropopause cold trap, and is therefore equal to 2% in the central flash-forming region. On the other hand, our

inversion of the model intensity profile assumes *no* opacity due to methane absorption, whereas Lellouch *et al.* (1986) attributed the 30% decrease in mean central flash intensity *entirely* to methane absorption, and for an isothermal model atmosphere ($T = 150^\circ\text{K}$ throughout), this would require a 1% methane mixing ratio. It seems that the correct model lies somewhere between these extremes; the temperature distribution could be similar to that of the model of Orton *et al.*, but the methane mixing ratio must then be smaller than 1%, so that methane opacity is not significant for the mean central flash intensity. It will eventually be desirable to combine the occultation-derived constraints on Neptune's stratosphere with other ground-based and spacecraft-based constraints to obtain a fully consistent model for Neptune's atmosphere.

Table V gives calculated sky-plane coordinates for immersion and emersion points, and corresponding values of $t_{1/2}$, as obtained from solution 1. These results are given for comparison with solution 3 and with Table II.

Solution 3

Table VI gives the coordinates on the sky plane corresponding to the times given in Table II. These coordinates are measured with respect to the corrected Neptune cen-

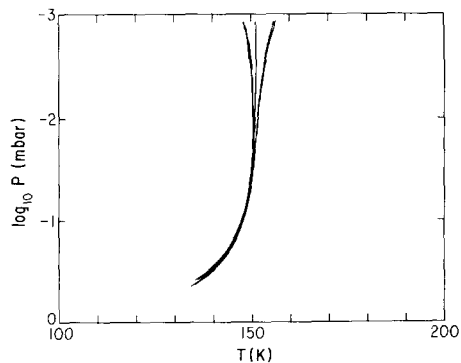


FIG. 4. Variation of T with pressure, as obtained from inverting Eq. (2).

TABLE V
PREDICTED HALF-INTENSITY TIMES AND
CORRESPONDING SKY-PLANE COORDINATES WITH
RESPECT TO NEPTUNE'S CENTER (NOT CORRECTED
FOR REFRACTIVE AND RELATIVISTIC BENDING),
FROM SOLUTION 1

Event	x (km)	y (km)	$t_{1/2}$ (UTC)
CTIO im.	-24,965	-2412	5 ^h 17 ^m 32 ^s .0
CTIO em.	25,109	141	6 ^h 35 ^m 00 ^s .4
ESO im.	-24,974	-2329	5 ^h 17 ^m 26 ^s .5
ESO em.	25,108	218	6 ^h 34 ^m 55 ^s .5
CFHT im.	-24,777	4315	5 ^h 28 ^m 16 ^s .4
CFHT em.	23,865	7453	6 ^h 41 ^m 16 ^s .9

ter coordinates (x_0, y_0) obtained from solution 1 (Table IV).

We carried out two versions of solution 3. In the first version, all of the points in Table VI were given equal weight. In the second version, points were given weights inversely proportional to the square of the timing uncertainties given in Table II. In both cases, the adjusted parameters were e ,

$\Delta x_0, \Delta y_0$, and a_0 , and p_n was held fixed at the value for solution 1 (20.1°). Results for solution 3, together with radial residuals Δr (observed - calculated), are given in Table VII.

An entirely independent astrometric solution to the limb data, which omitted the Mt. Wilson timings, yielded the results $a_0 = 25259 \pm 6$ km, $e = 0.0191 \pm 0.0012$, consistent with solution 3 (unequal weight version). After repeating the solution using Harris' nominal pole ($p_n = 22.9^\circ$; see below), the equatorial radius increased by 8 km, while e decreased to 0.0176 ± 0.0012 . Thus the constraint on p_n comes from the central flash data alone, while the limb-derived e is quite sensitive to p_n .

DISCUSSION

Uncertainties

We find, consistent with the results of Lellouch *et al.*, that the inferred scale height at the flash level H_f corresponds to a

TABLE VI
COORDINATES OF POINTS ON SKY PLANE
(UNCORRECTED FOR REFRACTION OR RELATIVISTIC
RAY BENDING)

Station	x (km)	y (km)
CTIO		
immersion	-24,968	-2413
central flash	-431	-1158
emersion	25,104	141
ESO		
immersion	-24,972	-2329
central flash	-402	-1077
emersion	25,107	218
IRTF		
immersion	-24,763	4315
emersion	23,861	7452
CFHT		
immersion	-24,773	4315
emersion	23,872	7453
Mt. Wilson		
immersion	-24,632	5098
emersion	23,710	7845
Lowell		
immersion	-24,619	5034
emersion	23,757	7733

TABLE VII
PARAMETERS OF SOLUTION 3

Parameter	Equal weights	Unequal weights
	Value	Value
e	0.0204	0.0195
Δx_0	+1 km	0 km
Δy_0	-29 km	-13 km
a_0	25,263 km	25,260 km
Station	Δr (km)	Δr (km)
CTIO im	2.4	2.4
CTIO em.	-2.5	-1.9
ESO im.	-2.4	-2.4
ESO em.	1.5	1.9
IRTF im.	-3.5	-4.7
IRTF em.	3.9	-5.2
CFHT im.	6.4	5.2
CFHT em.	14.6	5.6
Mt. Wilson im.	11.4	9.9
Mt. Wilson em.	-12.8	-22.4
Lowell im.	-14.2	-15.7
Lowell em.	-4.6	-14.1

temperature of about 100°K at a pressure of 240 μ bar. However, when allowance is made for the existence of a temperature gradient between the half-intensity region and the central flash region, the inferred scale height H_f actually corresponds to a temperature of about 135°K at a pressure of about 370 μ bar. If the actual temperature at this level is higher, then the transmission would need to be reduced from unity. But assuming no absorption along the optical path, the deepest inferred temperature and pressure point is in reasonable agreement with Appleby's (1986) Neptune model atmosphere. At the half-intensity points on the limb, the region probed by the rays has a scale height H_0 of 51 ± 4 km (average of results from fitting to immersion/emersion profiles), corresponding to a temperature of 150°K for solar-composition gas. The corresponding pressure is 1.0 μ bar. Table VII presents the oblateness e at this level in the atmosphere. Strictly speaking, in fitting a general model, allowance should be made for the variation of e with depth. We estimate the altitude difference between the 1- and the 400- μ bar level to be approximately 300 km, or 0.012 in units of a_0 . If we let

$$\eta = \frac{d \ln e}{d \ln r}, \quad (3)$$

where r is the radius in units of a_0 , then the surface value of η is given by hydrostatic-equilibrium theory (Zharkov and Trubitsyn 1978), assuming a constant rotation rate:

$$\eta = 3 - \frac{15 J_2}{2 e}, \quad (4)$$

where $J_2 = 0.004$ (Harris 1984) is the second-degree zonal harmonic of Neptune's gravity field. Employing Eq. (4), we find the oblateness at the flash level $e_f = 0.982 e$, where e is the oblateness at the 1- μ bar level. The intensity pattern in the central flash (solution 3) is primarily sensitive to e_f rather than to e . But comparing solution 3 (central flash fit only) with solution 2 (limb

fit only), we find that, formally, $e_f > e$. This discrepancy could be indicative of errors in the fitting procedure, ultimately traceable to deviations of the atmosphere from a state of perfect hydrostatic equilibrium. Such deviations could be local density irregularities which lead to redistribution of light in the shadow pattern (scintillation—see Hubbard *et al.* 1988), or they could be due to variations on a larger scale, such as a higher average scale height at the pole than at the equator.

Solution 1, which fits simultaneously to limb data and central flash data, should represent the best compromise between the various analyses presented here. Error bars in derived quantities, which are quoted in the abstract, are estimated from the differences between the various solutions.

Using the nominal Neptune pole position at the time of the occultation, computed from Harris' (1984) paper, we obtain $p_n = 22.9^\circ$ and $\beta_e = -25.0^\circ$. This position assumes that the angle ε between Neptune's rotation vector and the angular momentum vector of the Neptune-Triton system is -3.6° . If ε is taken to be zero, corresponding to negligible Triton mass, then Harris' ephemeris gives $p_n = 21.6^\circ$, $\beta_e = -21.7^\circ$. According to the results given in Table IV, the best-fit value of p_n from solution 1 is 20.1° . Considering that the error in the predicted pole position (for fixed Triton mass) is about $\pm 1.5^\circ$, this result is close to satisfactory agreement with Harris' pole position for zero Triton mass. However, we cannot thereby conclude that Triton's mass is much smaller than the nominal value since we have no constraint on β_e . Throughout this paper we use the value of β_e corresponding to the nominal Harris ephemeris, i.e., $\beta_e = -25.0^\circ$, although the value of p_n is adjusted to fit the central flash intensities and times observed at ESO and CTIO. The values of e given in Tables IV and VII and elsewhere in this paper thus correspond to $\beta_e = -25.0^\circ$. To within errors of order e^2 , the inferred oblateness scales as $(\cos \beta_e)^{-2}$. Thus if β_e were revised

to -21.7° from -25.0° , values of e given in this paper would have to be reduced by 5%.

The values of a_0 given in Tables IV and VII and elsewhere in this paper include a correction of +105 km for refractive and general-relativistic bending of the rays (Hubbard *et al.* 1985).

The principal test of consistency in our data set is the comparison of the parameters e and $\Delta x_0, \Delta y_0$ as derived from the three solutions. The discrepancy in the e 's is less than or equal to 7%, in agreement with the error bars assigned in Paper I and here. Similarly, the discrepancies in the derived centers of Neptune are about one scale height or smaller. Thus we conclude that the data set from the 1985 August 20 occultation are fully self-consistent and are adequately represented by the model.

Comparison with Previous Solutions

In this section, we compare the present results with those obtained from the 1983 June 15 Neptune occultation by Hubbard *et al.* (1985; H85) and by French *et al.* (1985; F85). In order to compare the results of this paper with previous investigations, we must adopt a consistent Neptune pole position for both the 1983 and 1985 observations. For this purpose, we assume that Harris' (1984) ephemeris with $\varepsilon = -3.6^\circ$ gives the correct value of β_e , but that the predicted value of p_n must be reduced by $\sim 2^\circ$. Then the oblatenesses derived by H85 and F85 change because of their correlation with p_n . The revised values of H85, $e = 0.023 \pm 0.004$, $a_0 = 25295 \pm 50$ km are consistent with the results of solution 1. The corrected F85 results, which also incorporated data from an occultation in April 1968, and for which a somewhat higher accuracy is claimed, are $e = 0.0200 \pm 0.0017$, $a_0 = 25255 \pm 12$ km. These are also consistent with solution 1.

Implications for Interior Structure

Is Neptune far less centrally condensed than Uranus, as claimed by F85? Let us review this question by first computing the

second-degree response coefficient Λ_2 for Uranus. This quantity is given by

$$\Lambda_2 = \lim_{q \rightarrow 0} J_2/q, \quad (5)$$

where

$$q = \omega^2 a_0^3 / GM, \quad (6)$$

ω is the planet's angular rotation velocity (assumed uniform), G is the gravitational constant, and M is the planet's mass. In Eq. (5), the second-degree zonal harmonic J_2 is normalized to a_0 . Neglecting terms of order q^2 , we approximate Eq. (5) by $\Lambda_2 \approx J_2/q$. For Uranus we use $J_2 = 3.352 \times 10^{-3}$ (Elliot 1982). For a rotation period of 16.31^h (Goody 1982), we would have $q = 0.0355$, but the recent Voyager 2 measurement of the rotation rate of the deep Uranian interior gives a rotation period of 17.24^h (Warwick *et al.* 1986), which implies $q = 0.0318$, and thus $\Lambda_2 = 0.105$ for Uranus. Elliot (1982) measured the oblateness of Uranus' atmosphere by occultation techniques and obtained $P = 15.5^h \pm 1.3^h$, which would imply $\Lambda_2 = 0.088 \pm 0.014$ if we ignore the Voyager period. Although the rotation rate of the deep interior determines J_2 , the rotation rate of the atmosphere together with J_2 fixes the oblateness of the atmosphere, and if the two rotation rates are unequal, one cannot obtain Λ_2 from the oblateness and J_2 alone.

For Neptune we employ the equation

$$\Lambda_2^{-1} = \frac{2e}{J_2} - 3, \quad (7)$$

recognizing that it is invalid if the atmosphere and interior rotate at different rates. Taking Harris' lower bound for J_2 and our upper bound for e , we obtain $\Lambda_2 = 0.103$, and thus $q = 0.0341$ and the rotation period $P = 14.4^h$. If we take Harris' upper bound for J_2 and our lower bound for e , we obtain $\Lambda_2 = 0.183$, $q = 0.0252$, $P = 16.9^h$. The latter values are compatible with the results of F85.

We conclude that despite improved error bars on Neptune's oblateness, there is still

substantial uncertainty in its degree of central condensation as measured by Λ_2 . There is significant evidence that Neptune is less centrally condensed than Uranus, in agreement with F85, but a definitive resolution of this matter must await a determination of the rotation period of Neptune's deep interior, as would be provided by a measurement of the rotation period of a magnetosphere. When significant differential rotation is present in a planetary atmosphere, as is apparently the case for Uranus, the oblateness may differ substantially from that corresponding to uniform rotation, for a fixed value of J_2 (Hubbard 1986). This may explain the substantial discrepancy between the Voyager value for Uranus' deep rotation period and Elliot's and Goody's values. It may also account for the discrepancy between the rotation period for Neptune which we obtain here, $P = 15.6^{\text{h}} \pm 1.2^{\text{h}}$, and the rotation period of 18.2^{h} proposed by Belton *et al.* (1981).

ACKNOWLEDGMENTS

We thank B. Grundseth for help in acquiring the IR acquisition chain at CFHT, B. Gregory for essential support at CTIO, and M. Standish for much assistance with Neptune ephemerides and star positions. Helpful comments on the manuscript by Fred Franklin and James Elliot are appreciated. NASA Grants NSG-7045 and NGL-05-002-140 provided support for much of the data analysis.

REFERENCES

- APPLEBY, J. F. 1986. Radiative-convective equilibrium models of Uranus and Neptune. *Icarus* **65**, 383-405.
- BELTON, M. J. S., L. WALLACE, AND S. HOWARD 1981. The periods of Neptune: Evidence for atmospheric motions. *Icarus* **46**, 263-274.
- ELLIOT, J. L. 1982. Rings of Uranus: A review of occultation results. In *Uranus and the Outer Planets* (G. E. Hunt, Ed.), pp. 237-256. Cambridge Univ. Press, Cambridge.
- FRENCH, R. G., P. A. MELROY, R. L. BARON, E. W. DUNHAM, K. J. MEECH, D. J. MINK, J. L. ELLIOT, D. A. ALLEN, M. C. B. ASHLEY, K. C. FREEMAN, E. F. ERICKSON, J. GOGUEN, AND H. B. HAMMEL 1985. The 1983 June 15 occultation by Neptune. II. The oblateness of Neptune. *Astron. J.* **90**, 2624-2638.
- GOODY, R. M. 1982. The rotation of Uranus. In *Uranus and the Outer Planets* (G. E. Hunt, Ed.), pp. 143-153. Cambridge Univ. Press, Cambridge.
- HARRIS, A. W. 1984. Physical properties of Neptune and Triton inferred from the orbit of Triton. In *Uranus and Neptune* (J. Bergstrahl, Ed.), pp. 357-373. NASA Conf. Publ. 2330.
- HUBBARD, W. B. 1986. On the oblateness and rotation rate of Neptune's atmosphere. In *The Jovian Atmospheres* (M. Allison and L. D. Travis, Eds.), pp. 264-269. NASA Conf. Publ. 2441.
- HUBBARD, W. B., H. P. AVEY, B. CARTER, J. FRECKER, H. H. FU, J.-A. GEHRELS, T. GEHRELS, D. M. HUNTEN, H. D. KENNEDY, L. A. LEBOSKY, K. MOTTRAM, T. MURPHY, A. NIELSEN, A. A. PAGE, H. J. REITSEMA, B. A. SMITH, D. J. THOLEN, B. VARNES, F. VILAS, M. D. WATERWORTH, H. H. WU, AND B. ZELLNER 1985. Results from observations of the 15 June 1983 occultation by the Neptune system. *Astron. J.* **90**, 655-667.
- HUBBARD, W. B., E. LELLOUCH, B. SICARDY, A. BRAHIC, F. VILAS, P. BOUCHET, R. A. MCLAREN, AND C. PERRIER 1988. Structure of scintillations in Neptune's occultation shadow. *Astrophys. J.* **325**, in press.
- LELLOUCH, E., W. B. HUBBARD, B. SICARDY, F. VILAS, AND P. BOUCHET 1986. Occultation determination of Neptune's oblateness and methane stratospheric mixing ratio. *Nature* **324**, 227-231.
- ORTON, G. S., D. K. AITKEN, C. SMITH, P. F. ROCHE, J. CALDWELL, AND R. SNYDER 1987. The spectra of Uranus and Neptune at 8-14 and 17-23 μm . *Icarus* **70**, 1-12.
- STANDISH, E. M., JR. 1982. Orientation of the JPL ephemerides, DE200/LE200, to the dynamical equinox of J2000. *Astron. Astrophys.* **114**, 297-302.
- WARWICK, J. W., D. R. EVANS, J. H. ROMIG, C. B. SAWYER, M. D. DESCH, M. L. KAISER, J. K. ALEXANDER, T. D. CARR, D. H. STAELIN, S. GULKIS, R. L. POYNTER, M. AUBIER, A. BOISCHOT, Y. LEBLANC, A. LECACHEUX, B. M. PEDERSEN, AND P. ZARKA 1986. Voyager 2 radio observations of Uranus. *Science* **233**, 102-106.
- ZHARKOV, V. N., AND V. P. TRUBITSYN 1978. *Physics of Planetary Interiors*. Pachart Press, Tucson, AZ.